Comparing different Jet-Algorithms for photoproduction Monte Carlo data

Clemens Mellein

DESY Hamburg / RWTH Aachen

Abstract. The following report shows the results of a comparison between the k_t, anti-k_t, Cambridge/Aachen and SISCone jet-algorithms, which were used to analyse direct and resolved dijet photoproduction Monte Carlo data from the Pythia event generator. For the leading jets we demanded cuts of 25, 15 and - if a third jet existed - 10 GeV. It was investigated if the results of each algorithm agree for the comparison between reconstructed- and hadron- level. To find corresponding jets on different levels a matching procedure was introduced, which depends on a goemetrical radius parameter. To optimize this and the radius parameter of the different jet algorithms is one of our main aims.

1. MOTIVATION

Jetalgorithms are one of the most important tools in high energy physics data analysis. They provide an opportunity to reconstruct the initiating partons and initiating processes of any complex events. But since the projection of a multiparticle bunch to a simple jet is fundamentally ambiguous - which reflects the variety of existing jetalgorithms - it is important to understand their characteristcs in defining the jets. Therefore we use Monte Carlo data from the Pythia event generator and compare the properties of the defined jets on hadron level with the properties of the jets on reconstructed level.

The HERA experiments aim on measuring the strong coupling α_s, proton PDFs and various cross sections $ep \rightarrow jets$. In case of photoproduction reactions, which are at least of $\mathcal{O}(\alpha\alpha_s)$, one can also study the PDF of the photon, which exhibits a hadronic structure in these special reactions. Therefore it is important to identify the best parameter settings of the used jetalgorithms for the special requirements of these experiments. Since in the last years a lot of new jetalgorithms like the anti-k_t and SISCone emerged, the interest in testing their characteristics is again growing.

(e-mail: Clemens.Mellein@rwth-aachen.de)

*Supervisors: Günter Grindhammer (guenterg@desy.de), Roman Kogler (kogler@desy.de), Aziz Dossanov (aziza@desy.de)

2. BASICS OF ELECTRON-PROTON-SCATTERING

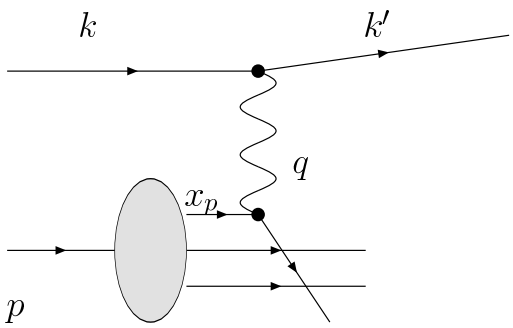

FIG 1. *Electron proton scattering process.*

In electron proton scattering reactions occur electromagnetic interactions, mediated by a photon, as well as weak interactions, mediated by the Z_0 (neutral currents) or the $W\pm$ (charged currents). The charged current interactions can easily be separeted by cutting on missing energies and momenta, carried away by the emerging neutrino. These scattering reactions (see figure 2) can be described by several sets of kinematical variables. Important variables are the

center of mass energy

$$s = (p+k)^2 \approx 4E_e E_p, \tag{2.1}$$

which is usually fixed at collider experiments. E_e is the electron energy, E_p the proton energy, this and all following approximations are valid in the high energy limes, when electron and proton masses can be neglected. The (negative) squared momentum transfer

$$Q^2 = -q^2 = -(k-k')^2 \approx 2E_e E'_e(1-\cos\theta) \tag{2.2}$$

is used to divide the interactions in further classes, like deep inelastic scattering (DIS) with high Q^2. A similar work on jet algorithms for DIS data has been done by B. Lemmer, see (5). In cases of vanishing Q^2 one speaks of *photoproduction* interactions, where a quasi real photon is exchanged. θ is the angle of the scattered electron relative to the beam axis, E'_e the energy of the scattered electron. In reactions $ep \to eX$ with fixed center-of-mass energy the kinematics can be fully described by two variables,

$$y = \frac{p\cdot q}{p\cdot k} \approx 1 - \frac{E'_e}{E_e}\sin^2\frac{\theta}{2}, \tag{2.3}$$

called the inelasticity of the process, which is in the proton rest frame equal to the energy loss of the scattering electron. The second variable is

$$x_p = \frac{q\cdot a}{q\cdot p}, \tag{2.4}$$

which can be interpreted as the momentum fraction of the scattering parton coming from the proton with four momentum a.

3. PHOTOPRODUCTION

As already mentioned, one speaks of photoproduction in cases of $Q^2 \approx 0$. The photon can either interact directly with one parton from the proton, which is called *direct photoporduction*, or it can fluctuate into quark-antiquark pairs or a vector meson, which is then interacting with one parton from the proton, this is called *resolved photoproduction*. The longitudinal momentum fraction of the photon-side parton is then defined by

$$x_\gamma = \frac{p\cdot b}{p\cdot q}, \tag{3.1}$$

with the parton momentum b, similar to the proton case (cf. equation 2.4). This means that the photon exhibits a hadronic structure and one of its partons is then participating in the hard interaction.

The usual approach to calculate photoproduction cross sections is to factorize them into one part that is calculable by perturbation theory, like electromagnetic and hard QCD processes, and a non perturbative part, where all soft QCD processes, for example radiation of soft gluons, are parametrized into so called structure functions, which are to be determined experimentally. Therefore we demand at least two hard jets to ensure that the parton interaction is on a hard scale, which is then calculable in pQCD. For the non perturbative processes in photoproduction we get two structure functions $f_p(\alpha_s, x_p, \mu_R, \mu_F)$ and $f_\gamma(\alpha_s, x_\gamma, \mu_R, \mu_F)$, one for the proton structure and the other one for the hadronic structure of the photon. In case of direct photoproduction the latter is not applicable, instead the electromagnetic coupling of the photon with the proton-side parton can be calculated in QED. The two structure functions depend on the strong coupling constant α_s, the proton-side and photon-side momentum fractions respectively, the renormalization scale μ_R and a factorization scale μ_F which defines a boundary for the processes, which are parametrized in the structure function. This is illustrated in figure 3. For the cross section for resolved events one gets then:

$$\begin{aligned} d\sigma^{res}_{ep} &= \sum_{i,j=q\bar{q}g}\int_0^1 dx_p dx_\gamma f_{i,\gamma}(\alpha_s, x_\gamma, \mu_R, \mu_F) \\ &\quad \times f_{j,p}(\alpha_s, x_p, \mu_R, \mu_F) d\sigma_{ij}(\alpha_s, px_p, qx_\gamma\mu_R) \end{aligned} \tag{3.2}$$

For direct envents:

$$\begin{aligned} d\sigma^{dir}_{ep} &= \sum_{i=q\bar{q}g}\int_0^1 dx_p f_{i,p}(\alpha_s, x_p, \mu_R, \mu_F) \\ &\quad \times d\sigma_i(\alpha_s, px_p, q\mu_R) \end{aligned} \tag{3.3}$$

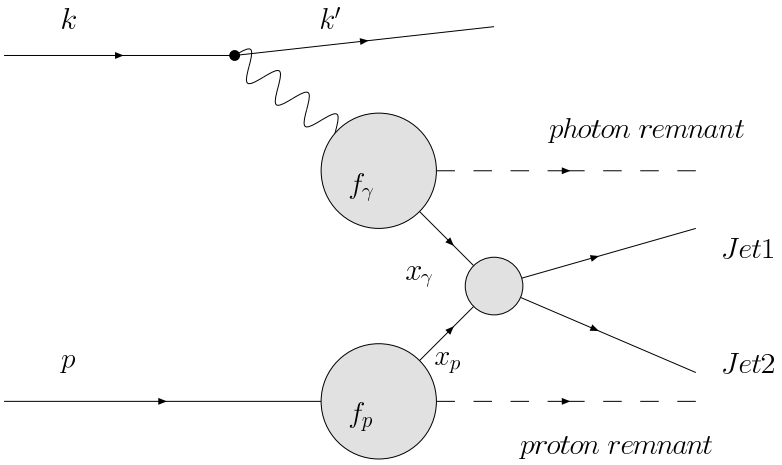

FIG 2. *Schematic view of dijet photoproduction process in ep-scattering. The small grey circle depicts the hard (short scale) parton-parton interaction.*

The leading order interactions of direct dijet photoproduction are QCD compton scattering $\gamma q \to gq$ and the so called photon-gluon-fusion $\gamma g \to q\bar{q}$, respectively, which are of $\mathcal{O}(\alpha\alpha_s)$ (cf. figure 3). There are various LO diagrams for the hard parton-parton interaction of the resolved photoproduction (depicted with a small grey circle in figure 3), which are of $\mathcal{O}(\alpha\alpha_s^2)$, e.g. processes like $q\bar{q} \to q\bar{q}$, $qq \to qq$. For these and NLO diagrams, virtual and real corrections, see (3).

4. JET ALGORITHMS

For all types of jet algorithms, one requires infrared and collinear safety, factorizability and a small renormalization scale dependence. This guarantees that the defined jets do not lead to divergent observables. Finally, all algorithms should give the same results, e.g. the same jet quantities, on all levels. On detector level one considers all objects recorded by trackers and calorimeters, which are later identified by their momenta and energies as certain particles (reconstructed level). This is the only known information after conducting an experiment. But what one wants to know, the physical truth, are the underlying processes between partons and hadrons (parton and hadron level).

In general, one can discriminate between two widespread classes of jetalgorithms, the sequential recombination algorithms (also called clustering algorithms), like k_t, anti-k_t and Cambridge/Aachen and the conetype algorithms, such as SISCone. Both classes of jetalgorithms are sensitive to different types of non-perturbative QCD corrections, cf. (1) and (2).

For the clustering algorithms some kind of like angular distance d_{ij} between two particles and a distance d_{iB} between a particle and the beam is introduced. The latter distance is used for a stopping criterion of the clustering process, as described further down. The algorithm then proceeds by identifying the minimal d_{ij} for a particle i and combining it with j, as long as d_{ij} is smaller than d_{iB}. If it is no longer smaller, i is defined as a jet. The merging of two particles is done due to the p_t-weighted scheme:

$$\begin{aligned} p_{t,ij} &= p_{t,i} + p_{t,j}, \\ \eta_{ij} &= \frac{p_{t,i}\eta_i + p_{t,j}\eta_j}{p_{t,ij}}, \\ \phi_{ij} &= \frac{p_{t,i}\phi_i + p_{t,j}\phi_j}{p_{t,ij}}. \end{aligned} \tag{4.1}$$

This merging scheme results in massless jets, which are ordered ascendently in p_t. The above described procedure is then repeated until no single entity is left. For the three recombination algorithms that we consider, the distances are defined by:

$$d_{ij} = \min\left(p_{t,i}^{2p}, p_{t,j}^{2p}\right)\frac{\Delta_{ij}^2}{R^2} \tag{4.2}$$

$$d_{iB} = p_{t,i}^{2p} \tag{4.3}$$

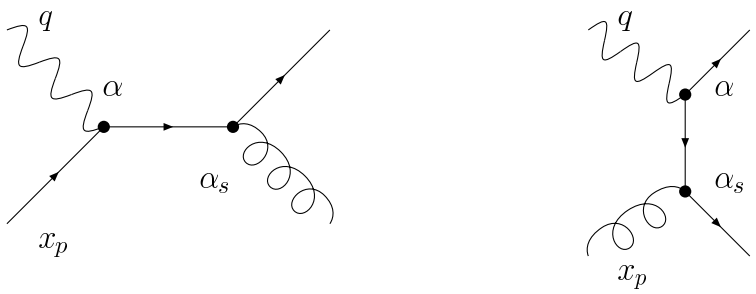

FIG 3. *Leading order diagrams of direct photoproduction with timelike or spacelike quark propagator.*

This definition for d_{ij} is composed of a relative power of energy scale, containing the transverse momenta of two jets, each to the power of $2p$, and a geometrical scale, which is governed by the radius parameter R, which is usually of $\mathcal{O}(1)$. The distance Δ_{ij} is defined by:

$$\Delta_{ij}^2 = (\eta_i - \eta_j)^2 + (\phi_i - \phi_j)^2, \tag{4.4}$$

the so called pseudorapidity η is related to the angle θ of a jet via

$$\eta = -\ln\left(\tan\frac{\theta}{2}\right). \tag{4.5}$$

It is in the high energy limes with negligable particle masses numerically close to the rapidity y defined in special relativity as

$$y = \frac{1}{2}\ln\frac{E + P_z}{E - P_z}. \tag{4.6}$$

It will be one of our main aims to find a good value for the parameter R for each jetalgorithm. Considering the parameter p, the case $p = 1$ corresponds to the k_t algorithm, $p = 0$ to the Cambridge/Aachen algorithm and $p = -1$ to the anti-k_t algorithm. The sign of the parameter p affects the ordering of the jets, considering a hard particle and a soft particle, for positive p the d_{ij} is dominated by the momentum of the soft paritcle and the geometrical distance, in contrast, in the case of negative p d_{ij} is dominated by the momentum of the hard particle and the geometrical distance, for the special case p=0 only the geometrical distance of the particles is relevant. A detailed description of the clustering behaviour of the anti-K_T algorithm you can find in (1).

The general idea of conetype algorithms is to define jets as a cone around certain directions with high energy flows. Also in this case a geometrical parameter R appears, in this case it is the radius of "trial" cones, which are put around certain seed-particles in the considered event. Then for each seed the sum of the four momenta of all particles in the cone is calculated, which yields a new direction for the trail cone. If the direction of a trail cone no longer changes after a certain amount of iteration steps, the cone is reffered to as "stable cone". Obviously the sum of the for momenta of all particles in a stable cone then has to coincide with the cone axis. Unfortunately, for the algorithms using seeds problems like infrared and collinear unsafety may occur. A way out of these problems is provided by seedless cone algorithms, like the SISCone algorithm. For more details about this algorithm see (2).

5. THE MONTE CARLO DATA

The Monte Carlo data used for this analysis is created with the Pythia 6.4 event generator (6) and contains 5 million direct and resolved photoproduction events. Multiple interactions between the resolved photon and the proton are not included in this data set, although Pythia allows to generate such processes. The data is fully simulated and reconstructed, so that a comparison between jets on reconstructed and generated jets on hadron level is possible.

6. PHASESPACE DEFINITIONS

For this work we consider photoproduction events with at least two hard jets, their transverse momen-

tum is demanded to be greater than 25 GeV and 15 GeV, respectively. These cuts ensure that the parton parton interaction is on a hard scale so that the cross section is calculable with the means of pQCD. If a third jet occurs, also here a cut of 10 GeV is applied. These p_t cuts are equal on hadron and reconstructed level, see table 1 and 2. The η cuts apply for all of the first three jets[1] and are also the same on both levels, we demand η to be in the range of $-0.5 < \eta < 2.75$, which is due to the constricted acceptance of the detector. To remove DIS events we require that there is no electron candidate found during the reconstruction, which restricts the photon virtuality to Q^2 <4 GeV, according to the detector acceptance of HERA II (cf. the relation between Q^2 and the angle θ of the scattered electron in equation 2.2). An equal cut on Q^2 is explicitly applied on hadron level. The cuts on the jet masses on rec-level have the purpose to remove any fake jet events, which occur when an electron is reconstructed as a jet after the detector simulation. Real jets have usually masses greater than 2 GeV. Charged currents are excluded due to a cut on missing p_t, which has to be below 20 GeV. Since $E - P_z$ is related to y_{JB} via $y_{JB} = \frac{E-P_z}{2E_e}$ the cuts on these quantities correspond to each other on the rec- and had-level.

A cut on the z-vertex position and the non-ep-background finding algorithms are usually used to remove cosmics, but is not necessary in the analysis of Monte Carlo data, since cosmics are not part of the simulation. Anyway, for the sake of completeness we take them in here.

For more details on photoproduction cuts and the above mentioned non-ep-background finders see (4).

TABLE 1
Phasespace definition. Cuts on reconstructed level.

parameter	*Cut*
z-vertex pos.	-35 cm$< z <35$ cm
$p_{t,miss}$	<20 GeV
$E - P_z$	5.52 GeV$< E - P_z <$49.68 GeV
no scattered electron	
$p_{t,1}$	>25 GeV
$p_{t,2}$	>15 GeV
$p_{t,3}$	>10 GeV
$\eta_{all\ jets}$	$-0.5 < \eta < 2.75$
$M_{jet,1}$	>2 GeV
$M_{jet,2}$	>2 GeV

[1]The labels 1st, 2nd and 3rd are due to the transverse momentum ordering of the jets.

TABLE 2
Phasespace definition. Cuts on hadron level.

parameter	*Cut*
Q^2	<4 GeV^2
y_{JB}	$0.1 < y < 0.9$
$p_{t,1}$	>25 GeV
$p_{t,2}$	>15 GeV
$p_{t,3}$	>10 GeV
$\eta_{all\ jets}$	$-0.5 < \eta < 2.75$

7. RESULTS

7.1 Jet Matching

To compare jets at reconstructed and hadron level, we had to introduce some matching procedure, which yields a pair of jets that is reasonable to compare. To this end, we yust calculated the geometrical distance $\Delta R^2 = (\Delta\eta)^2 + (\Delta\phi)^2$ for the three hardest had-jets to each of the five hardest rec-jets, the minimal distance was taken as matching criterion. We also introduced a boundary parameter ΔR[2], which excludes all rec-jets as a matching partner that have a greater distance to a certain had-jet than the given value. We calculated the matching efficiency, the ratio of the number of all matched jets to all matching trails, for different values of ΔR to find a parameter region, where the matching effienciency is better than 90% and the sensititvity of the efficiency with respect to the radius parameter of the jetalgorithms is low. A too large ΔR would lead to accidental mismatchings, so that a comparison between the different levels would be impossible. A too small ΔR would lead to a small matching efficiency and low statistics in all further analysis. We chose $\Delta R = 0.1$ to make a compromise.

Figures B,B and B show the matching efficiency for a fixed value of $\Delta R = 0.1$ plotted versus p_t and the angles η and ϕ. In the ϕ plot should no structure be recognizable, which is obviously confirmed by figure B. But the latter also reflects very clearly the stronger dependency of the k_t algorithm on R_0 compared to the anti-k_t. The other two algorithms do not show any peculiar behaviour in terms of the jet matching. In figure B one can recognize that the efficiency falls off for bigger values of η. Due to the lower detector precision in the forward direction there may be some weird mergings of jets or particles, so that

[2]Dont confuse it with the radius parameter R_0 of the jetalgorithms.

the resulting jets on rec-level can not match with them on had-level, whereby the matching efficiency finally decreases. In B one can see that the efficiency is increasing with increasing p_t, which is due to the better defined jets at high p_t, they then form a narrower bunch. This is also reflected in figures B, B and B, where the matching efficiency is plotted for each of the first three jets versus ΔR. The efficiency considerably decreases for the 2nd and 3rd had-jet.

7.2 Comparison between reconstructed and hadron level jet quantities

To compare reconstructed and hadron level we use the above described matching procedure for each had-jet. Then, for example, for every 1st had-jet the difference in p_t, η and ϕ between this jet and its matching jet on rec-level is plotted in a Root TH2D (see 7.2) versus its p_t, η, ϕ or the invariant mass of the first two had-jets M_{12}^2 on the x-axis. Afterwards, we calculate for each x-Bin the mean value and sigma of the particular difference distribution and fill them into new histograms. By this means one gets a clear view on the differences between the hadron level and reconstructed level jet definitions of each algorithm and for different radius parameters.

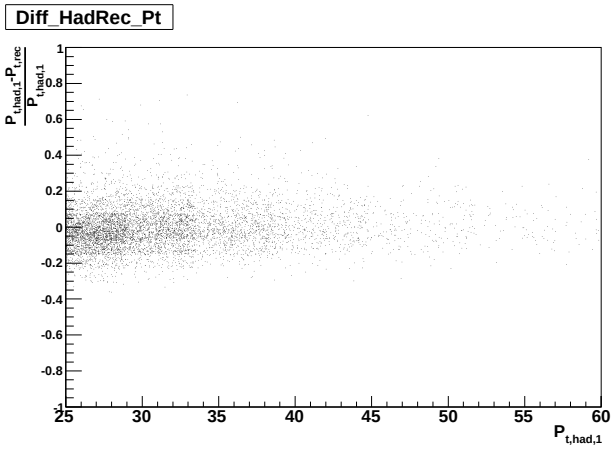

FIG 4. *Shown is, as an example, the 2dim distribution of the difference in p_t between the 1st had-jet and its matching jet on rec-level on the y-axis versus the 1st had-jets p_t on the x-axis. For each x-Bin we calculated then the mean value and the sigma of this distribution and filled it into separated histograms (shown on the next pages) to get a clear view on the differences between the hadron level and reconstructed level jet definitions of each algorithm. Used algorithm: k_t with $R_0 = 1.0$*

- **p_t histograms (figures in appendix C):** in terms of the p_t difference between rec- and had-level, bigger radii seem to improve the matching between the two levels, at least for high p_t of the first had-jet. In this field, the SIScone shows the worst performance, k_t and anti-k_t should be preferred here, as they show the smallest differences between rec- and had-level p_t. In terms of the η difference, Cambridge/Aachen and anti-k_t are a little more sensitive to changes in R_0 than the other two algorithms. All algorithms show here a positive offset, which gets smaller with decreasing R_0, except for SISCone. Also noticeable is the negative offset in the ϕ difference, which one would not expect. It means that the jetalgorithms repeatedly find the jets on had-level at higher ϕ values. All algorithms with all radii show this anomaly in a similar way, one will find it also in all following plots in a similar order of magnitude (≈ -0.005). So far, there is no explanation for it.
- **η histograms (figures in appendix D):** in terms of the p_t difference, again bigger radii seem to improve the matching between the two levels. The peculiar behaviour of all algorithms in the range of $\eta = 1.5$ is due to the transition between central and forward tracking detector. k_t and anti-k_t exhibit a slightly better behaviour than the other algorithms. In terms of the η difference, SIScone seems to have the best characteristics, as it shows the smallest deviation form 0 (especially for high η) and smaller dependencies on changes in R_0. In contrast, k_t, anti-k_t and Cam/Ac show higher dependencies on changes in R_0 and bigger deviations from 0, especially for high η. All algorithms exhibit a bigger η on had-level than on rec-level, but here only in the range of $\eta > 1$. This may also be related to the transition between central and forward tracking detector, which was already mentioned. This could explain the offset in η in the p_t histograms. The offset in ϕ is very similar for all algorithms, but not constant like in the p_t histograms. Instead, it is growing bigger from $\eta \approx 1$ on.
- **ϕ histograms (figures in appendix E):** as for the p_t difference, a radius of $R_0 = 1.0$ seems to be the best choice for all algorithms. The

k_t shows here and for the η difference the best performance. For the η differences, small radii improve the performance of all algorithms. The offset in ϕ is again very similar for all algorithms and radii.

- M_{12}^2 **histograms (figures in appendix F):** the behaviour seems to be very similar to the p_t plots. For M_{12}^2 less than 3000 GeV^2 the difference between hadron level and reconstructed level p_t is less than 0. In this region, smaller R_0 should be preferred for all jetfinders. In the region M_{12}^2 >3000 GeV^2 bigger radii yield better results. The first bin with lowest M_{12}^2 should not be considered too important in all plots, due to low statistics. In terms of the η difference, SISCone again seems to be slightly less dependent on changes in R_0.

7.3 Comparison with the results of the DIS analysis

Comparing this work with B. Lemmers analysis on DIS data (4), one first recognizes the lower matching efficiencies. This is due to the lower p_t cuts (first jet p_t >7 GeV) compared to the cuts in photoproduction. Since lower p_t jets are less precise defined, also the efficiency decreases. The behaviour of the matching efficiency versus p_t and η seems to be similar. The ϕ plots differ because of the boost into Breit frame apllied in B. Lemmers work. The offset in ϕ in the difference plots is also present in the DIS work, which means that also there the ϕ on rec-level is bigger than the ϕ on had-level. Interestingly, the offset is smaller for Rapgap data. The other results are hard to compare because of the different cuts on p_t and different Q^2 range. But in general, also in the DIS work k_t and anti-k_t seem to have a slightly better performance.

8. FINAL CONCLUSION AND OUTLOOK

The analysis shows that especially for k_t and anti-k_t $R_0 = 1.0$ is in most cases a good choice. SISCone in contrast works better with bigger radii. Cambridge/Aachen shows in most cases a slightly worse performance than the other algorithms. The behaviour of anti-k_t in terms of the jet matching is noticeable, here it shows the best efficiency, k_t in contrast shows the worst. One can conclude from that, that k_t and anti-k_t are the preferable algorithms, but all in all the differences between the jetfinders are rather small.

The mysterious offset in all ϕ difference histograms needs further investigations, a correction in the detector simulation and reconstruction process might be necessary.

Further studies of the differences between hadron and parton level and the separate consideration of direct and resolved photoproduction events might be interesting.

ACKNOWLEDGEMENTS

During my stay at DESY I had an interesting insight into scientific life and work. I want to thank Günter, Roman, Aziz, Adil and Zuzana from the H1 collaboration for all their help and the support during our work. Also thanks to my fellow summerstudent Boris Lemmer for the great entertainment during the work and life at DESY. Thanks to the fat, lazy cats lying all the time in front of the guesthouses and thus helping to create an enjoyable and inspiring atmosphere. Thanks also to the DESY snack and coffee machines for the reliable supply with all the things that are indispensable to life. Many thanks also to the organizers of the summerprogram, especially to Joachim Meyer and Andrea Schrader. Thanks to the lecturers for filling up our brains with huge amounts of physical knowledge. And finally I want to thank all the other summerstudents for the funny and pleasant time at DESY with all the parties, barbecues and city-tours. It was awesome! I like it!

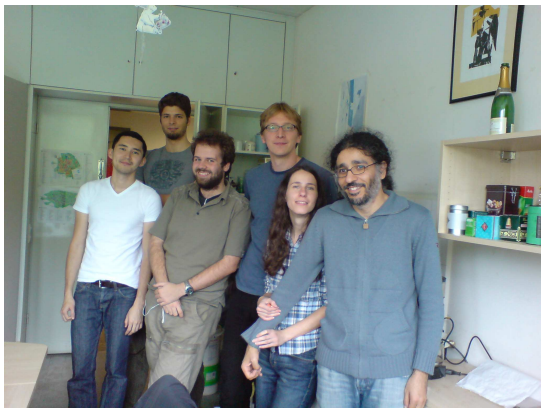

FIG 5. *My working group was really great!*

REFERENCES

[1] Matteo Cacciari and Gavin P. Salam. *The anti-k_t jet clustering algorithm.* JHEP 0804 (2008) 063 [arXiv:0802.1189]

[2] Gavin P. Salam and Gregory Soyez. *A practical seedless infrared-safe cone jet algorithm.* JHEP 05 (2007) 086 [arXiv:0704.0292]

[3] S. Caron. *Jets in photoproduction at HERA.* PhD thesis, RWTH Aachen 2002, DESY-THESIS-2002-035

[4] I. Strauch. *Jets with high transverse momenta in photoproduction at HERA.* PhD thesis, Universität Hamburg 2004, DESY-THESIS-2004-047

[5] B. Lemmer. *Comparing different jetalgorithms for DIS at high Q^2.* DESY summerschool 2008 student report.

[6] Torbjorn Sjostrand et. al. *PYTHIA 6.4 physics and manual.* JHEP 05 (2006) 026

APPENDIX B: JET MATCHING PLOTS

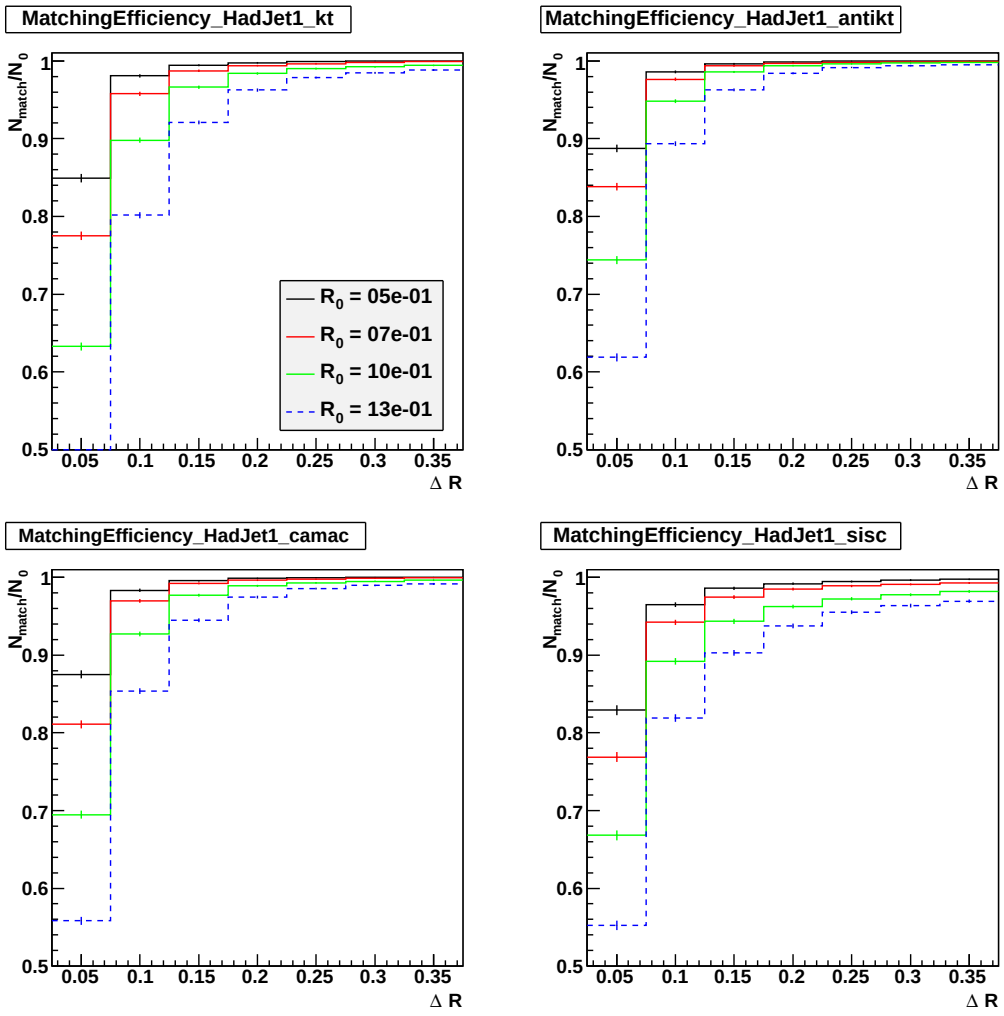

FIG 6. *1st jet on hadron level: matching efficiency for all jetalgorithms with different radius parameters (colored lines). The k_t algorithm seems to be more sensitive to changes in R_0 than the anti-k_t algorithm. The errors are calculated according to a binomial distribution of N_{match}*

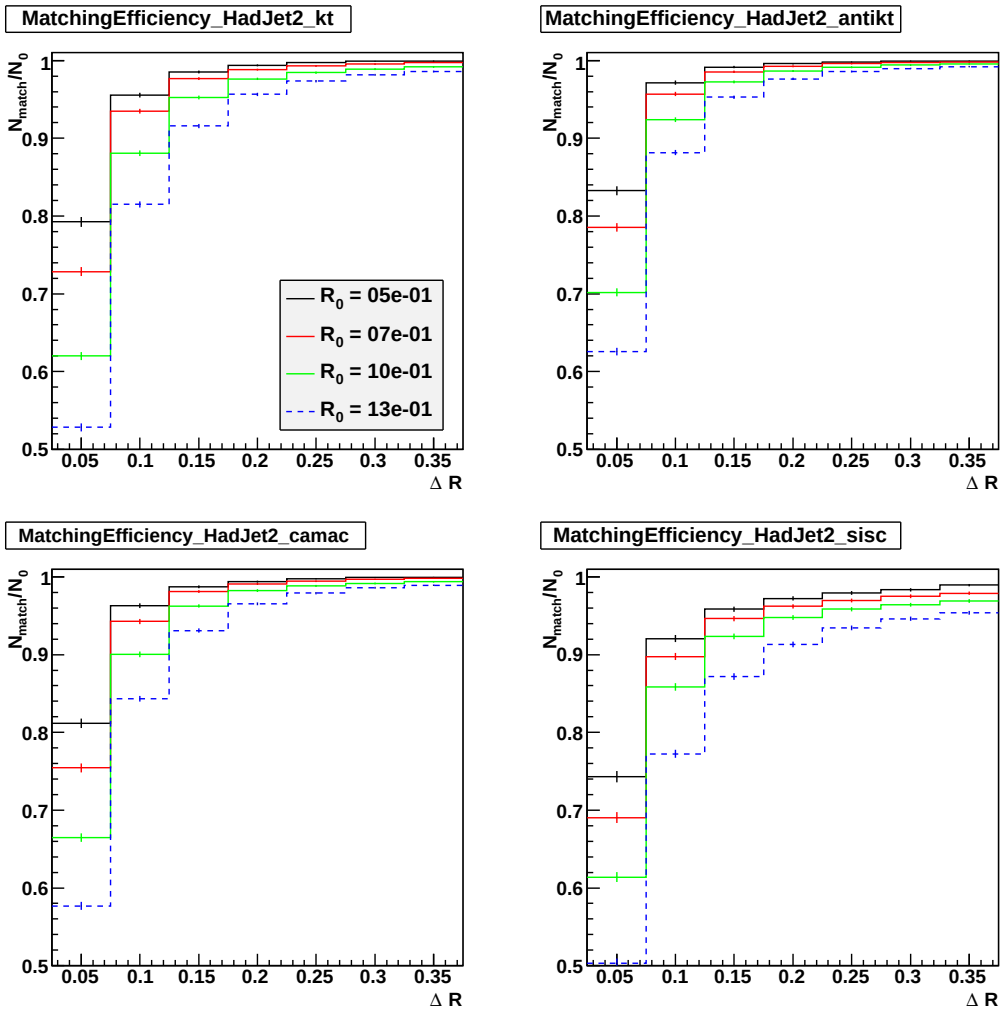

FIG 7. *2nd jet on hadron level: matching efficiency for all jetalgorithms with different radius parameters (colored lines). The errors are calculated according to a binomial distribution of* N_{match}

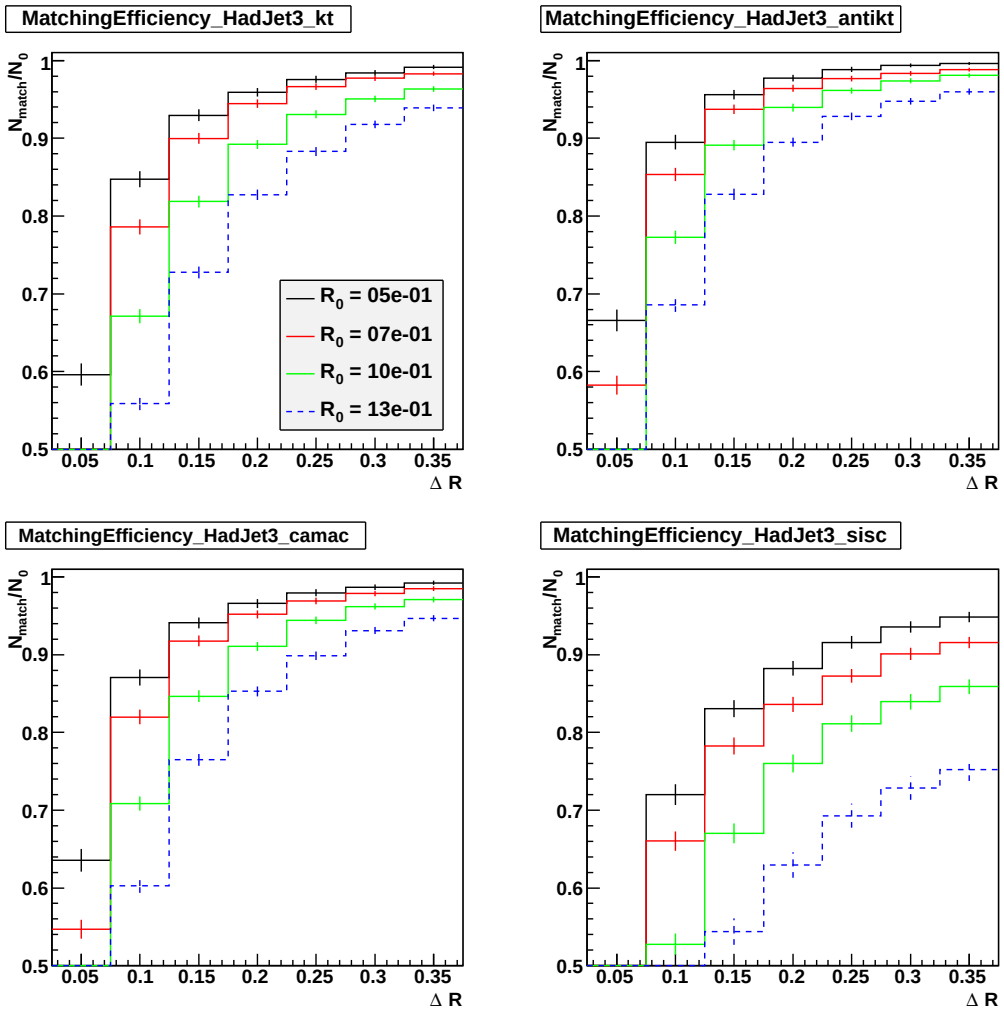

FIG 8. *3rd jet on hadron level: matching efficiency for all jetalgorithms with different radius parameters (colored lines). The errors are calculated according to a binomial distribution of* N_{match}

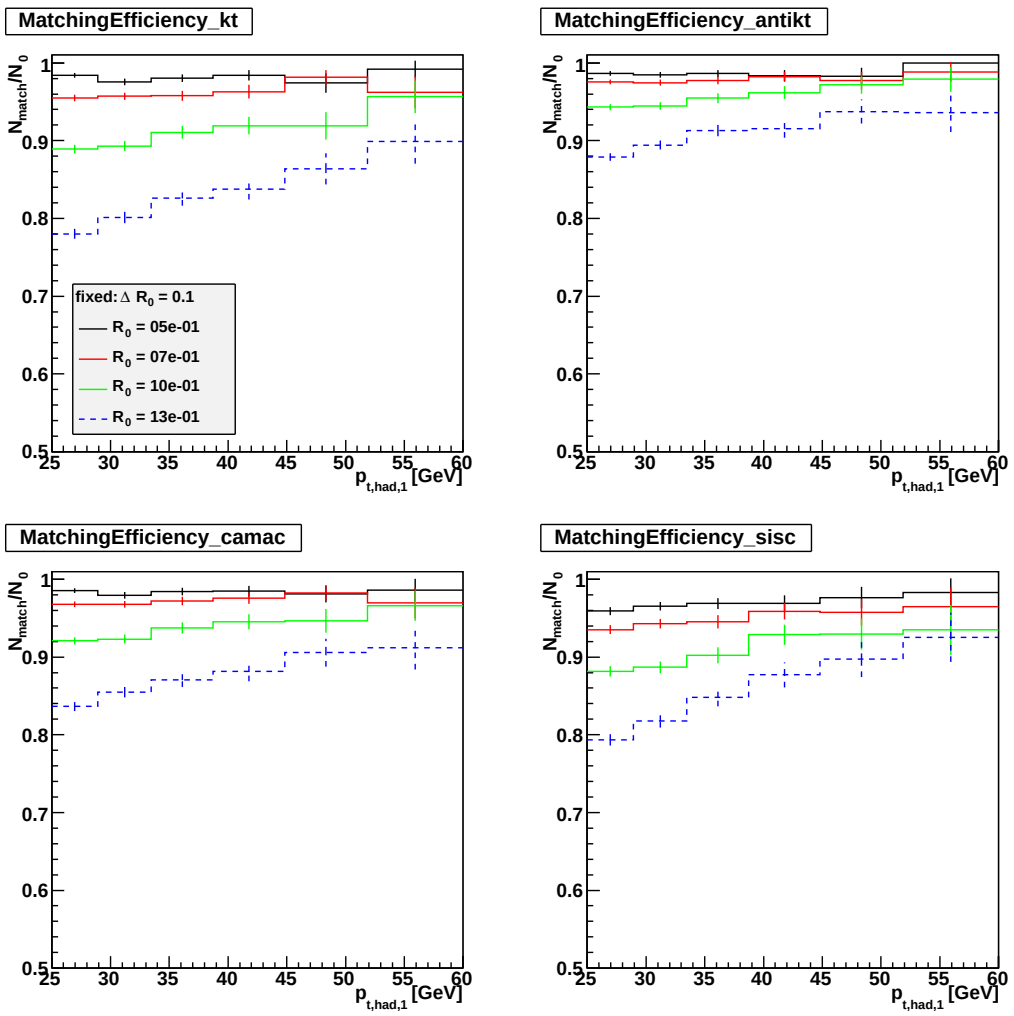

FIG 9. *1st jet on hadron level: matching efficiency for all jetalgorithms with different radius parameters (colored lines). The parameter* $\Delta R = 0.1$ *is here fixed, the matching efficiency is plotted versus the* p_t *of the 1st had-jet. The errors are calculated according to a binomial distribution of* N_{match}

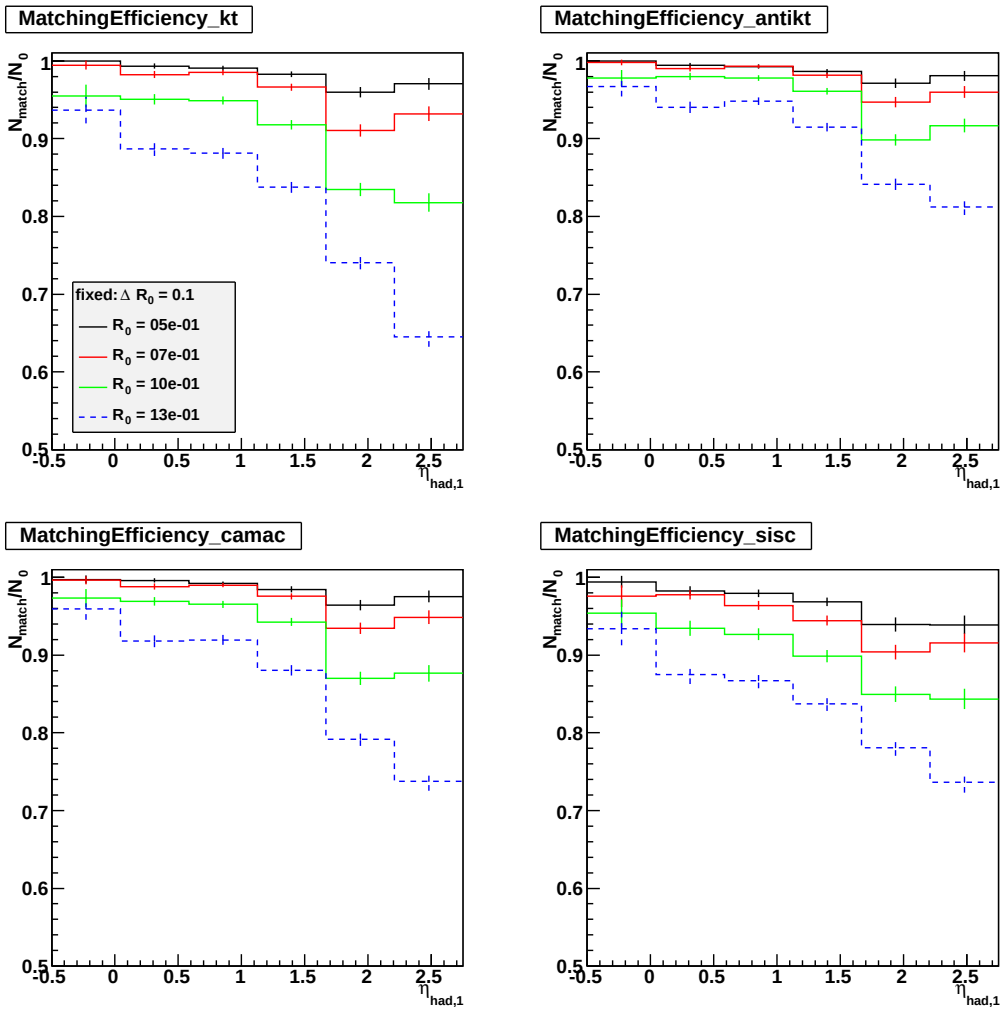

FIG 10. *1st jet on hadron level: matching efficiency for all jetalgorithms with different radius parameters (colored lines). The parameter* $\Delta R = 0.1$ *is here fixed, the matching efficiency is plotted versus the* η *of the 1st had-jet. The errors are calculated according to a binomial distribution of* N_{match}

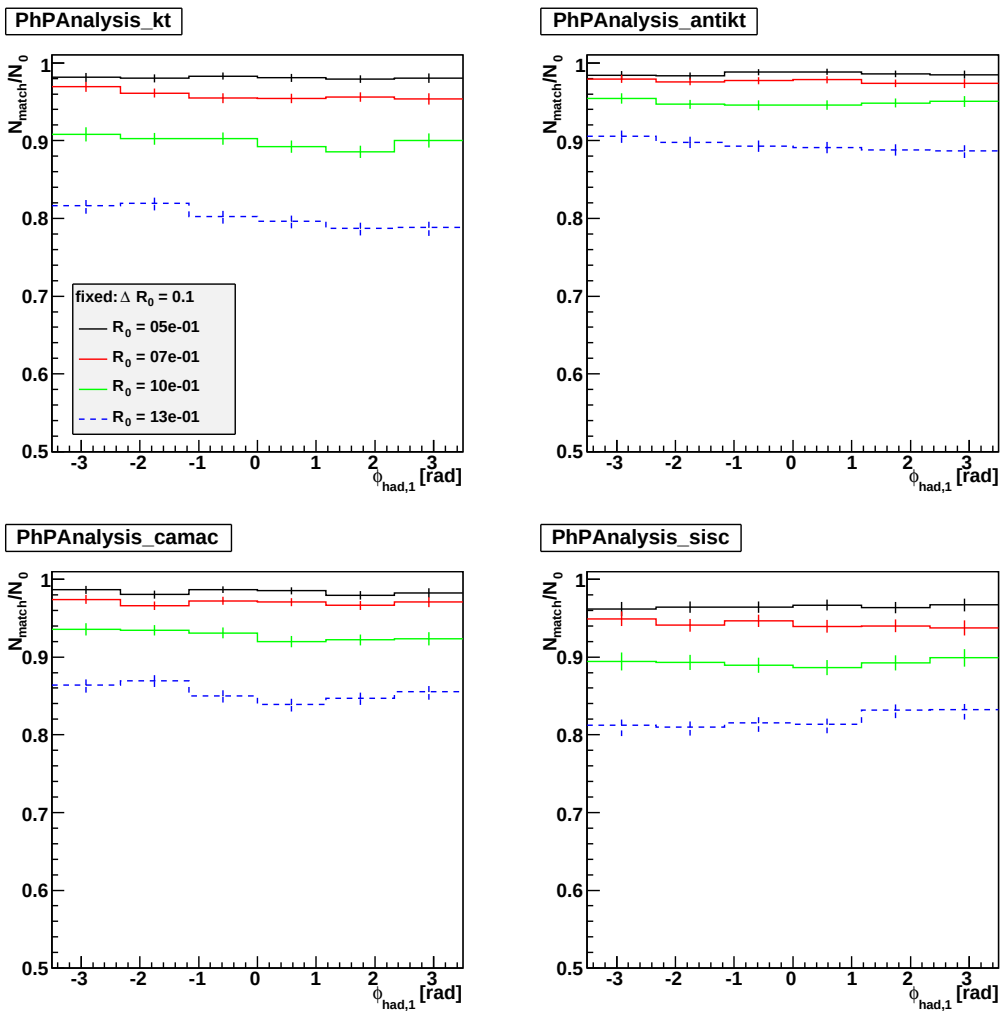

FIG 11. *1st jet on hadron level: matching efficiency for all jetalgorithms with different radius parameters (colored lines). The parameter* $\Delta R = 0.1$ *is here fixed, the matching efficiency is plotted versus the* ϕ *of the 1st had-jet. The errors are calculated according to a binomial distribution of* N_{match}

APPENDIX C: REC-HAD-LEVEL DIFFERENCES VERSUS $P_{T,HAD,1}$

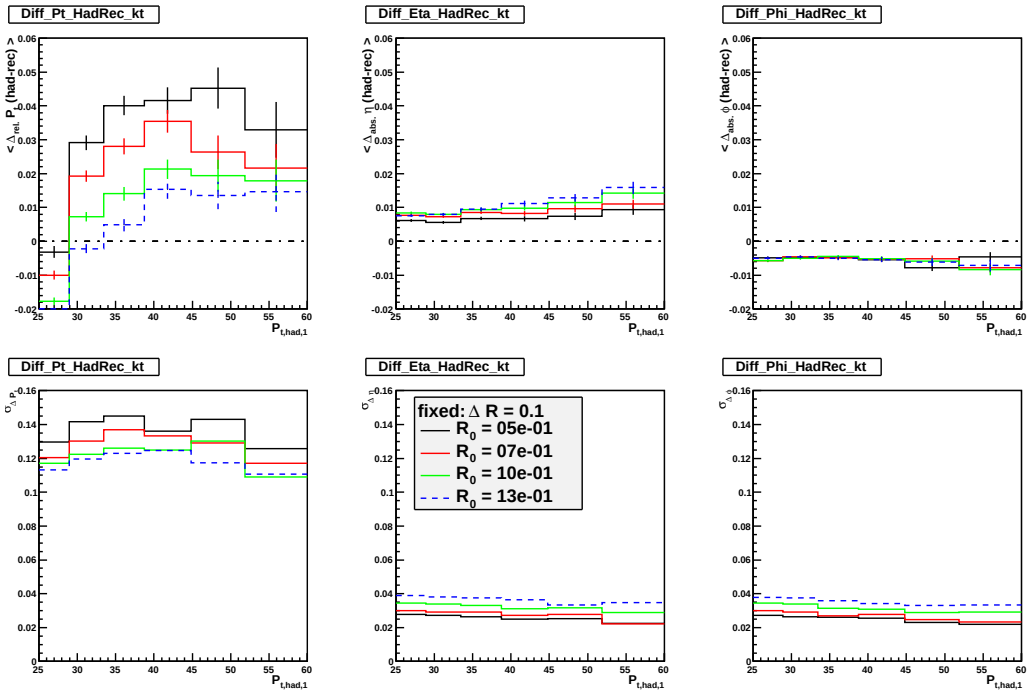

FIG 12. *In the first row, the mean values of the difference distributions between had- and rec-level are shown versus p_t of the first jet. The second row shows the associated sigmas of the difference distributions. The first column shows the difference in p_t, the second one the difference in η and the third one the difference in ϕ. Note that for the two angular quantities the absolute differences between had- and rec-level were calculate, whereas the p_t difference is calculated relative to the had-level p_t of the jet. Used jetalgorithm is k_t.*

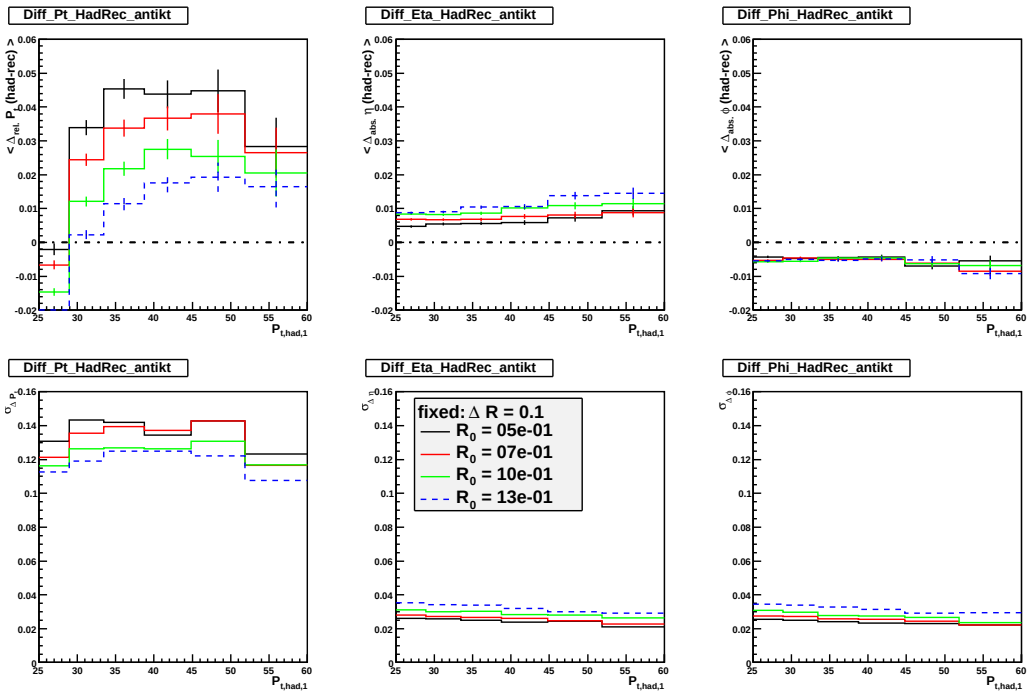

FIG 13. *Used jetalgorithm is anti-k_t.*

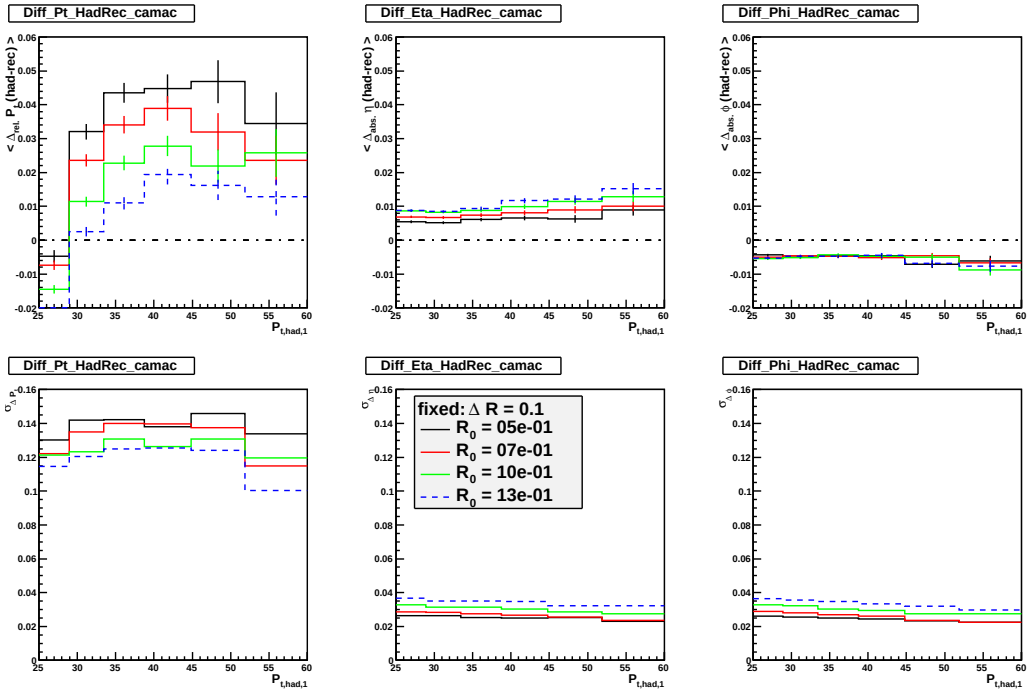

FIG 14. *Used jetalgorithm is Cambridge/Aachen.*

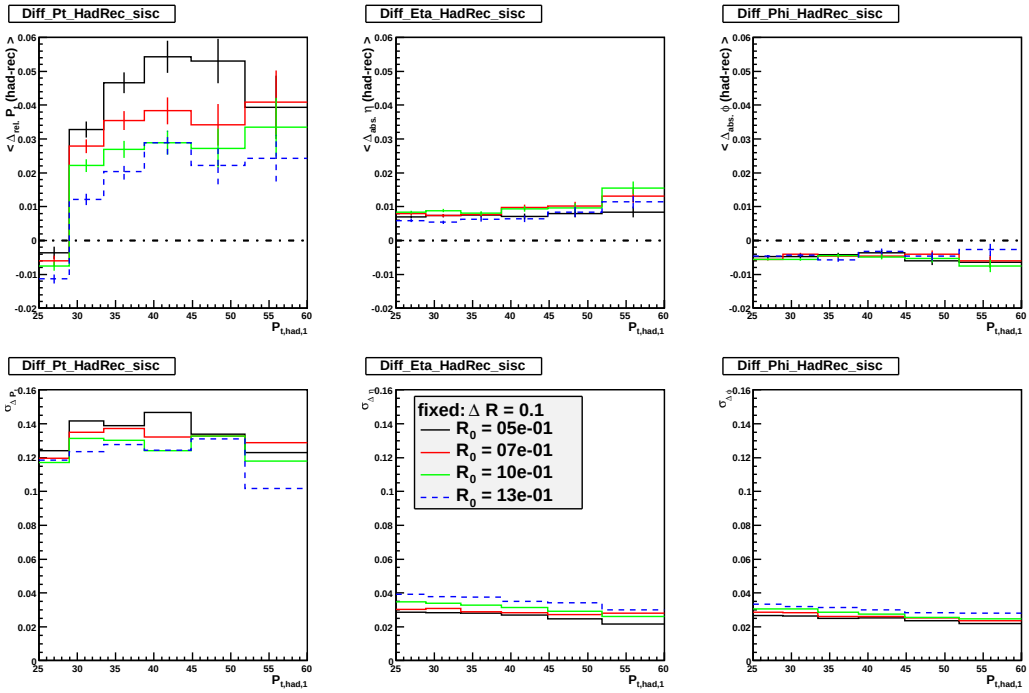

FIG 15. *Used jetalgorithm is SISCone.*

APPENDIX D: REC-HAD-LEVEL DIFFERENCES VERSUS $\eta_{HAD,1}$

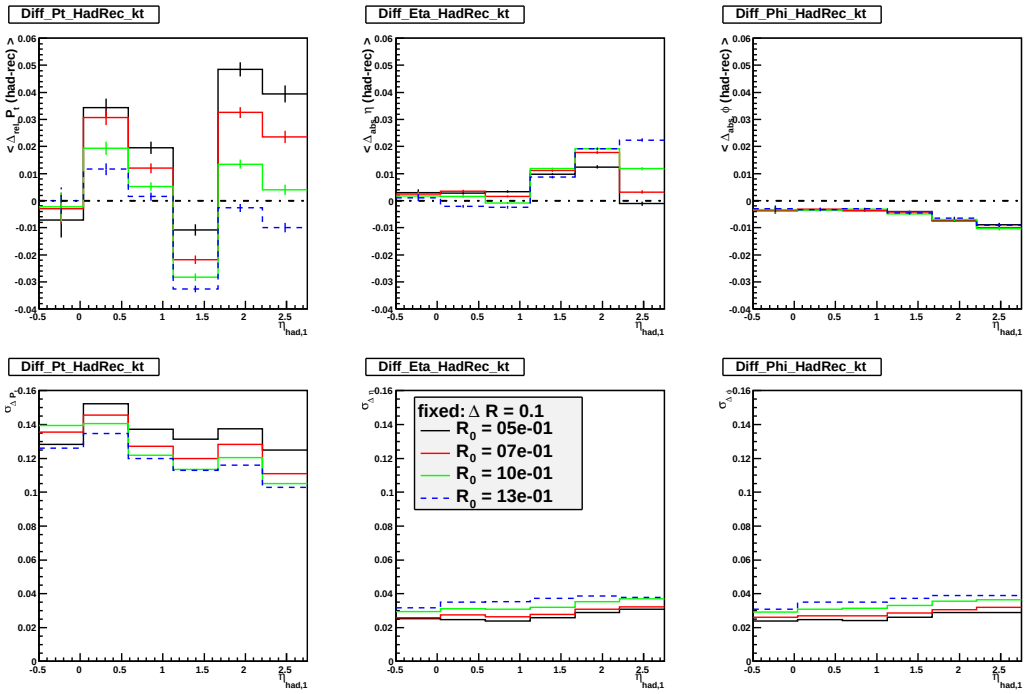

FIG 16. *In the first row, the mean values of the difference distributions between had- and rec-level are shown versus η of the first jet. The second row shows the associated sigmas of the difference distributions. The first column shows the difference in p_t, the second one the difference in η and the third one the difference in ϕ. Note that for the two angular quantities the absolute differences between had- and rec-level were calculate, whereas the p_t difference is calculated relative to the had-level p_t of the jet. Used jetalgorithm is k_t.*

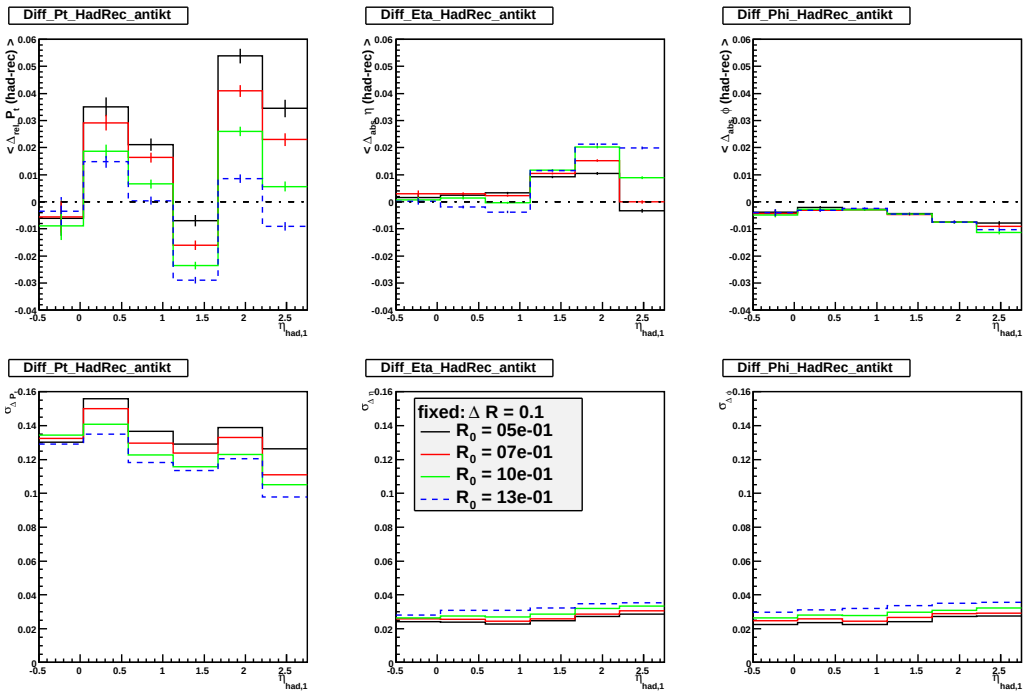

FIG 17. *Used jetalgorithm is anti-k_t.*

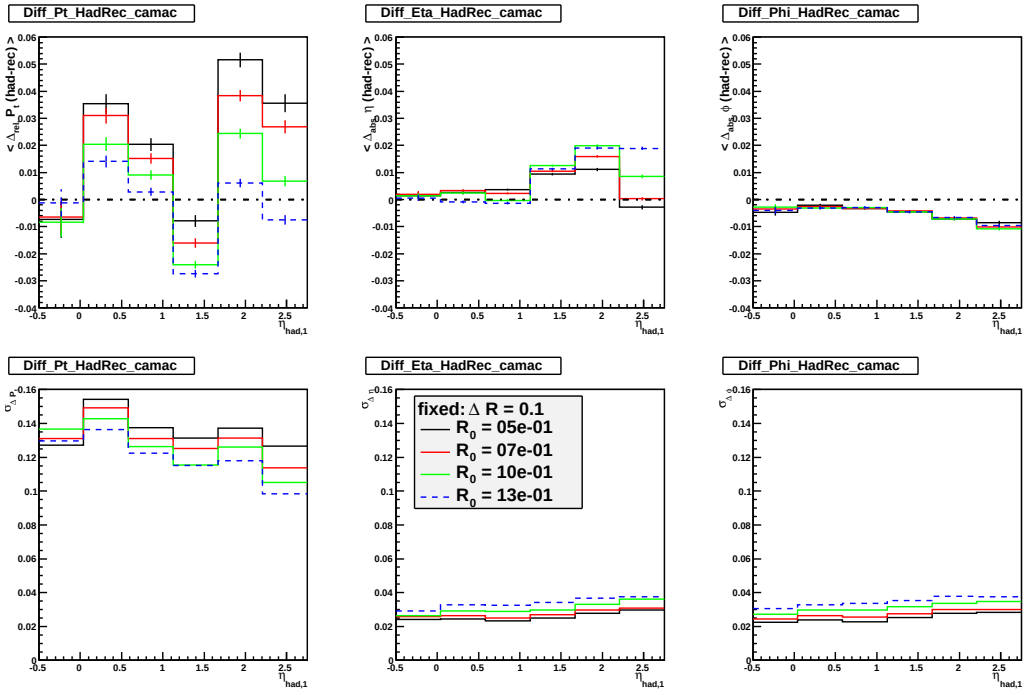

FIG 18. *Used jetalgorithm is Cambridge/Aachen.*

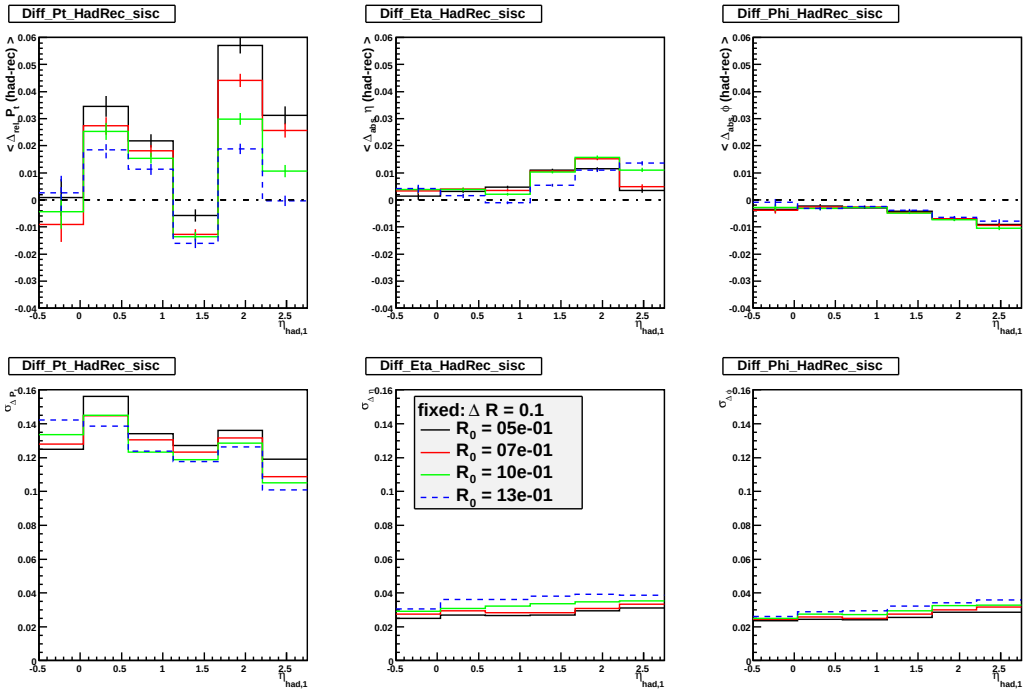

FIG 19. *Used jetalgorithm is SISCone.*

APPENDIX E: REC-HAD-LEVEL DIFFERENCES VERSUS $\phi_{HAD,1}$

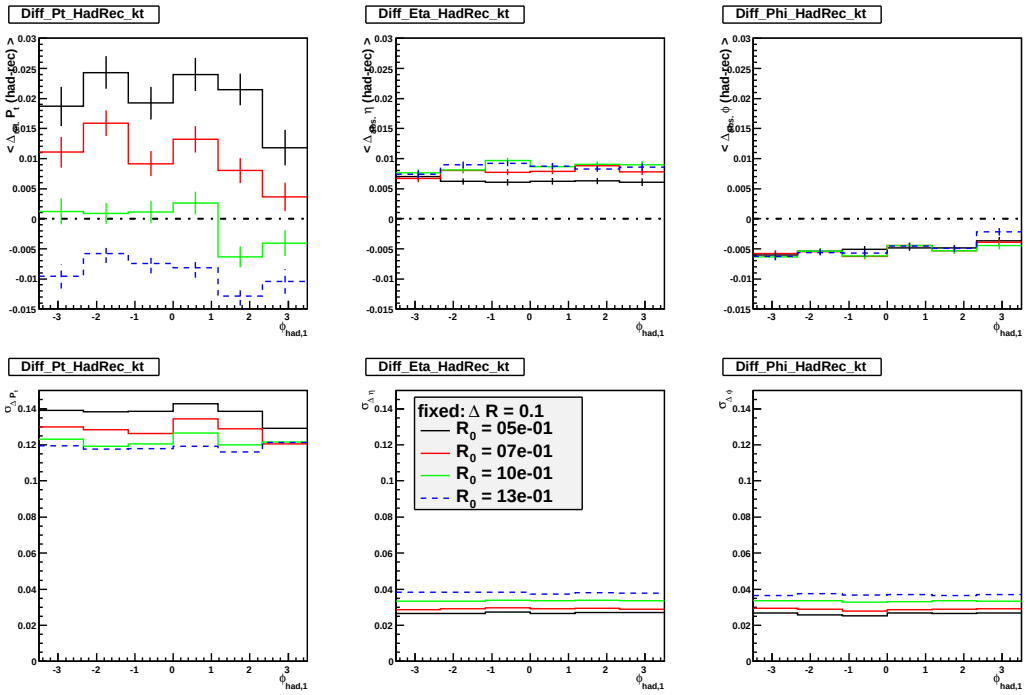

FIG 20. *In the first row, the mean values of the difference distributions between had- and rec-level are shown versus ϕ of the first jet. The second row shows the associated sigmas of the difference distributions. The first column shows the difference in p_t, the second one the difference in η and the third one the difference in ϕ. Note that for the two angular quantities the absolute differences between had- and rec-level were calculate, whereas the p_t difference is calculated relative to the had-level p_t of the jet. Used jetalgorithm is k_t.*

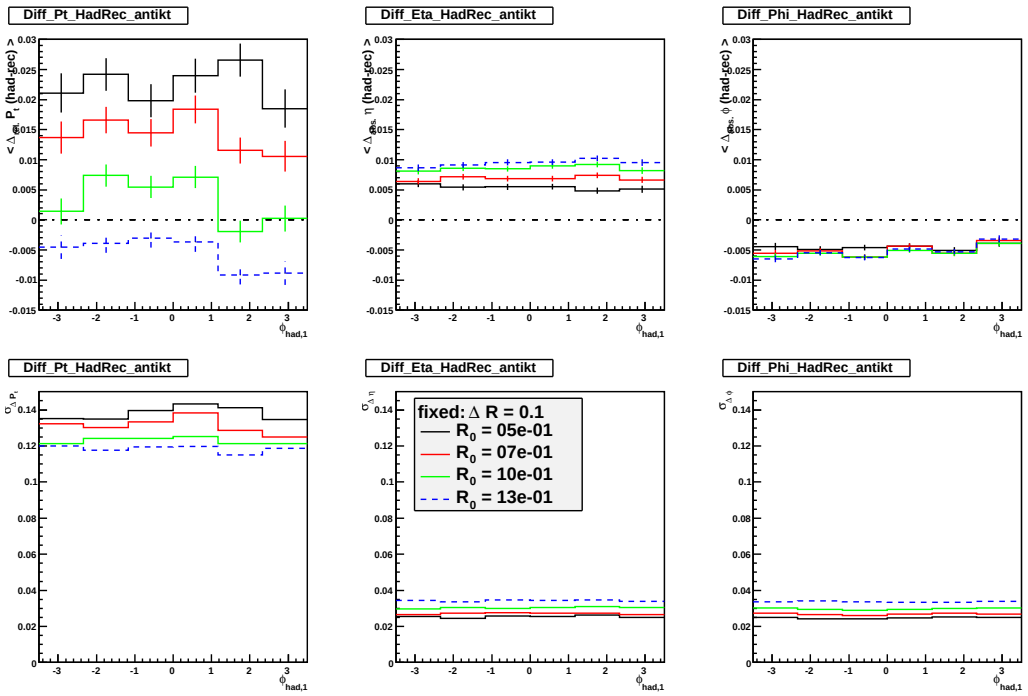

FIG 21. *Used jetalgorithm is anti-k_t.*

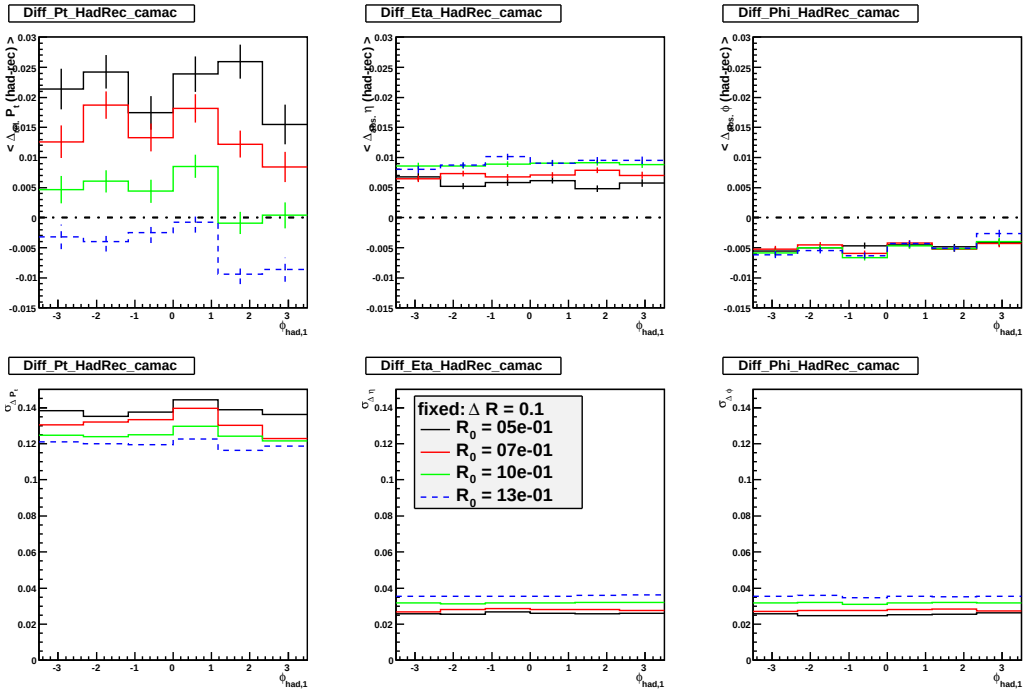

FIG 22. *Used jetalgorithm is Cambridge/Aachen.*

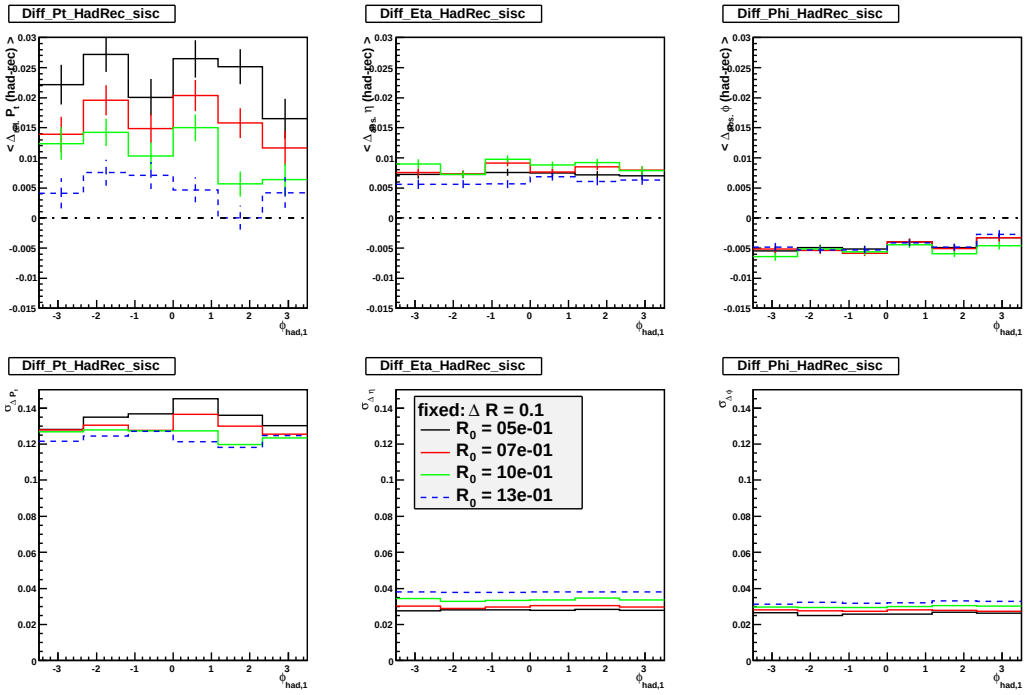

FIG 23. *Used jetalgorithm is SISCone.*

APPENDIX F: REC-HAD-LEVEL DIFFERENCES VERSUS $M^2_{HAD,12}$

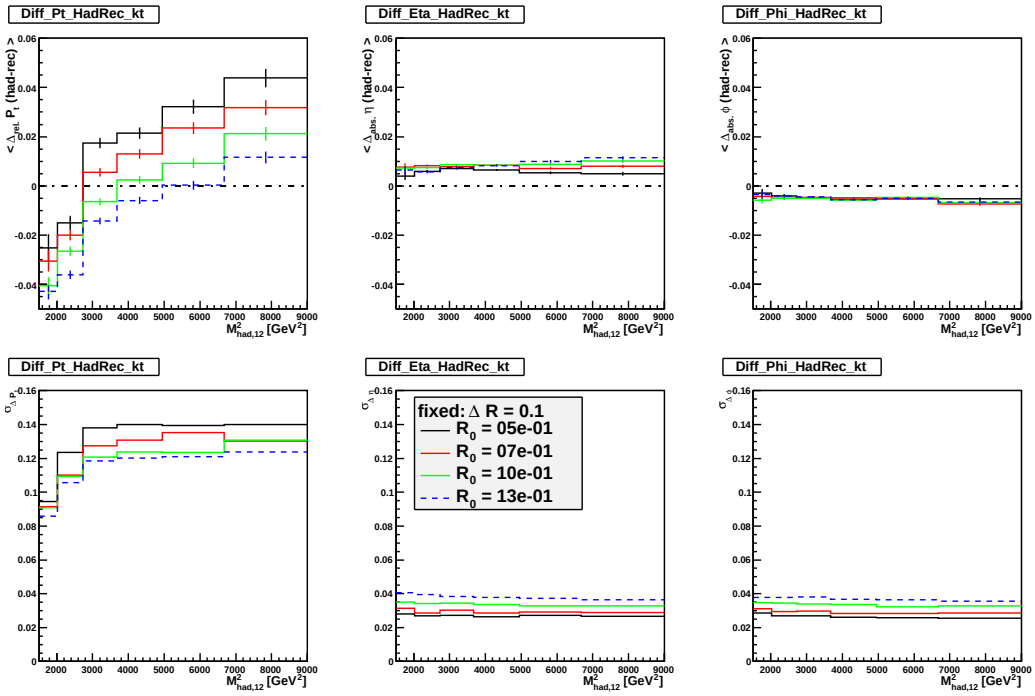

FIG 24. *In the first row, the mean values of the difference distributions between had- and rec-level are shown versus M^2_{12} of the first jet. The second row shows the associated sigmas of the difference distributions. The first column shows the difference in p_t, the second one the difference in η and the third one the difference in ϕ. Note that for the two angular quantities the absolute differences between had- and rec-level were calculate, whereas the p_t difference is calculated relative to the had-level p_t of the jet. Used jetalgorithm is k_t.*

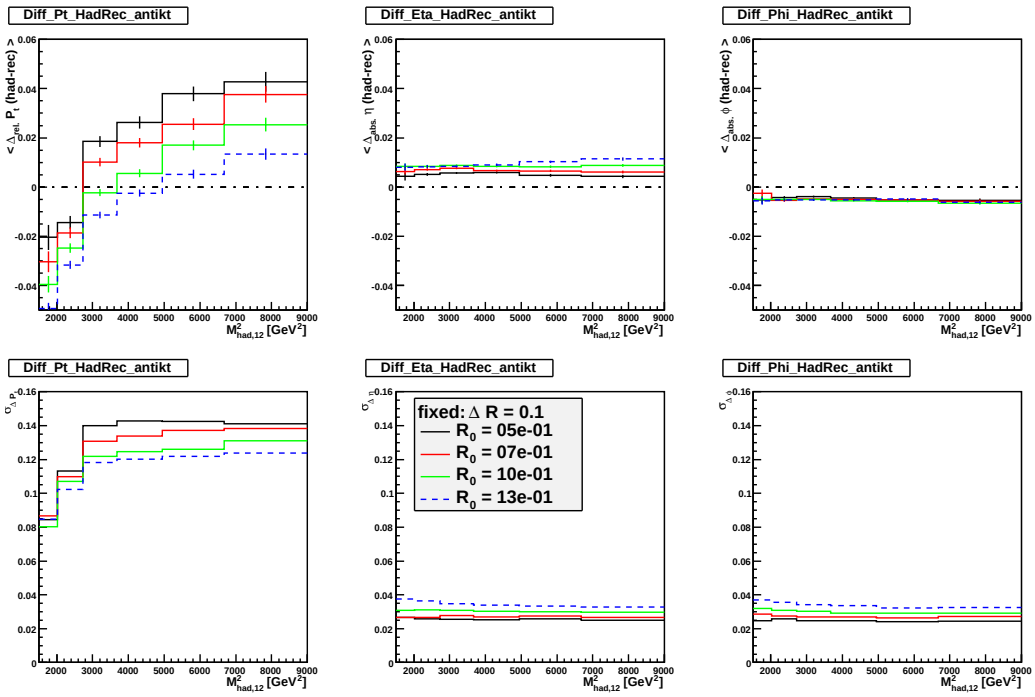

FIG 25. *Used jetalgorithm is anti-k_t.*

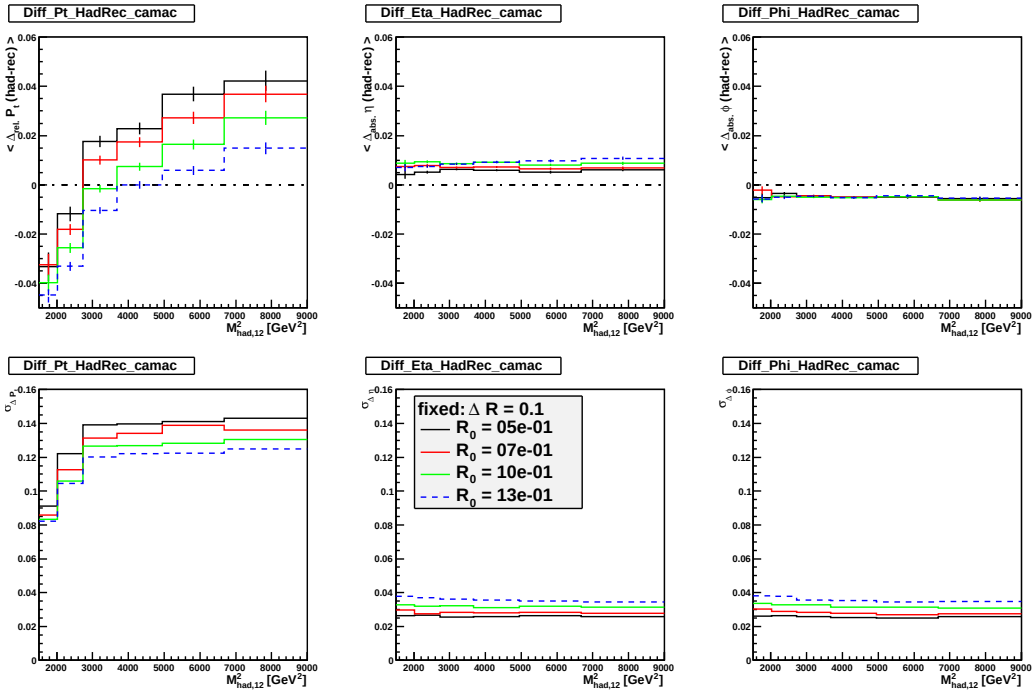

FIG 26. *Used jetalgorithm is Cambridge/Aachen.*

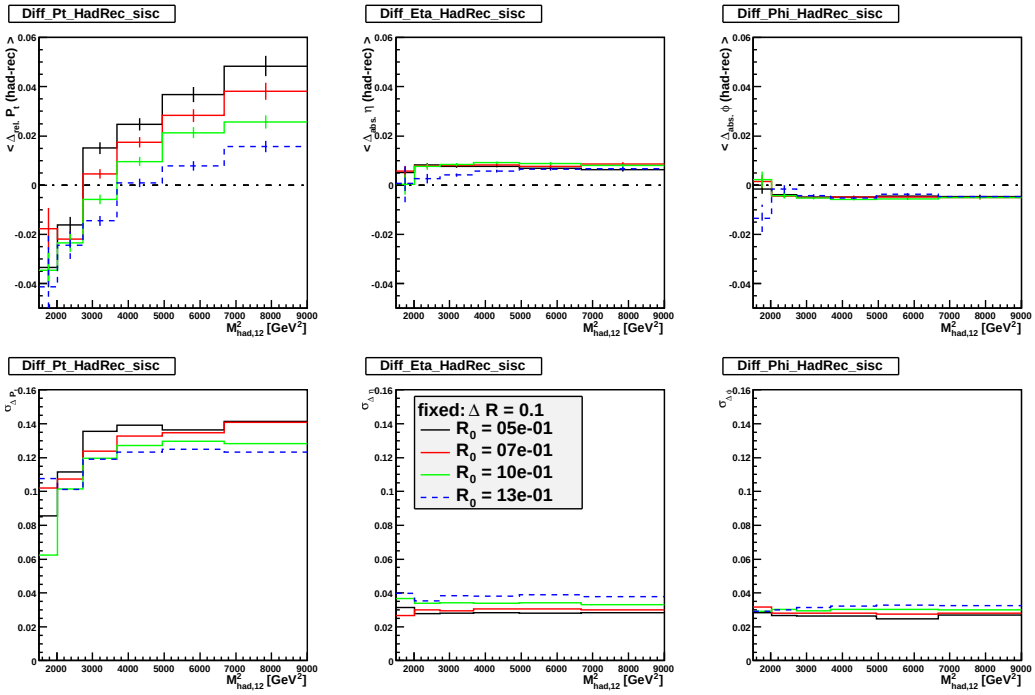

FIG 27. *Used jetalgorithm is SISCone.*